Supporting Information

Designing Multi-component Metal-organic Frameworks with Hierarchical Structure-mimicking Distribution for High CO_2 Capture Performance

Tong Xu,[a] Mingwei Jia,[a] Xin Liu,[b] Jiantang Li[a] and Yunling Liu[a]**

[a] State Key Laboratory of Inorganic Synthesis and Preparative Chemistry, College of Chemistry, Jilin University, Changchun 130012, P. R. China. E-mail: lijt1992@163.com; yunling@jlu.edu.cn.

[b] Department of Chemistry, Dalian University of Technology, Dalian 116024, P. R. China

Table of Contents

S1 Supporting Figures

Structure of JLU-MOF107

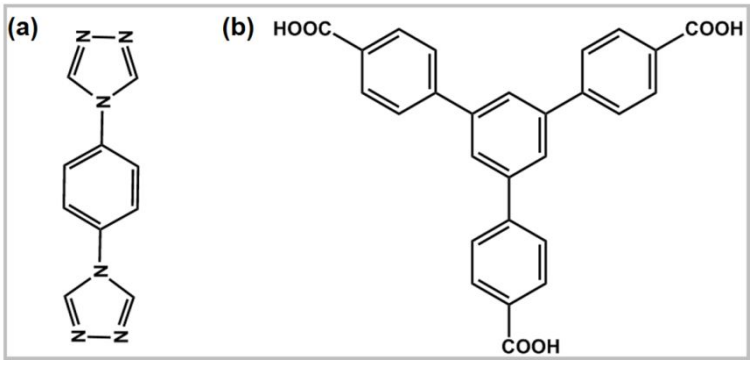

Figure S1. The p-tr$_2$ph (1,4-phenylene-4,4'-bis(1,2,4-triazole)) ligand (a) and (b) BTB (4,4',4''-benzene-1,3,5-triyl-tribenzoate) ligand.

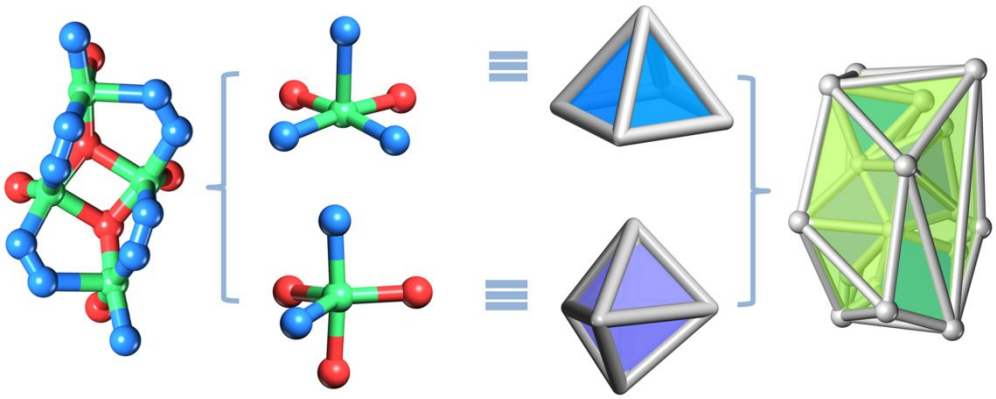

Figure S2. SBU-2 consisted of two different coordination modes of Cu(II). (C: light gray; O: red; N: blue; Cu: green.)

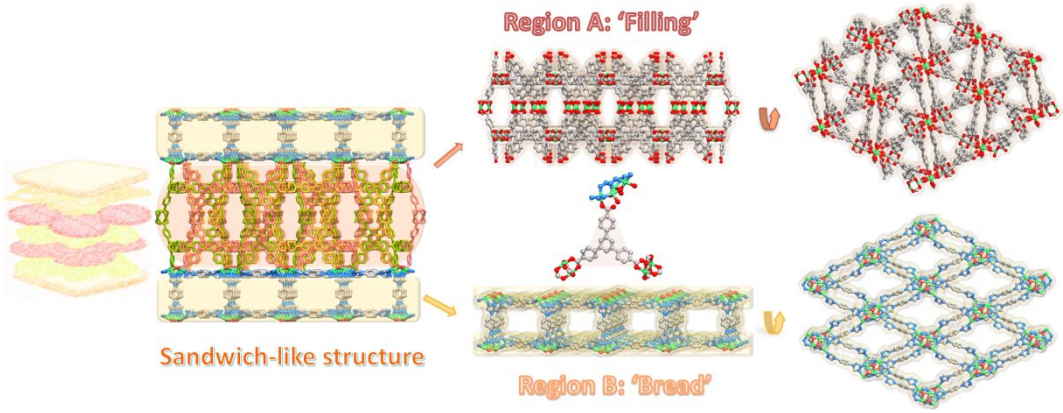

Figure S3. The sandwich-like structure: region A is a 3-fold interpenetrated layer of "filling" and region B is a pillared-layer of 'bread'.

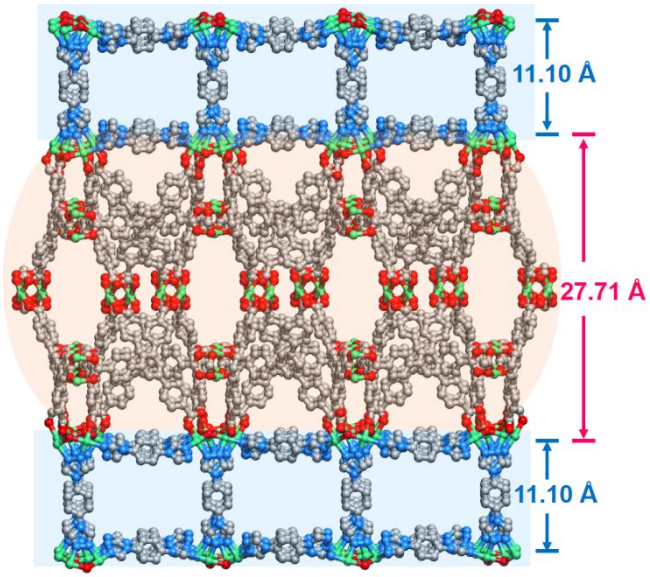

Figure S4. The distances between the unique layers.

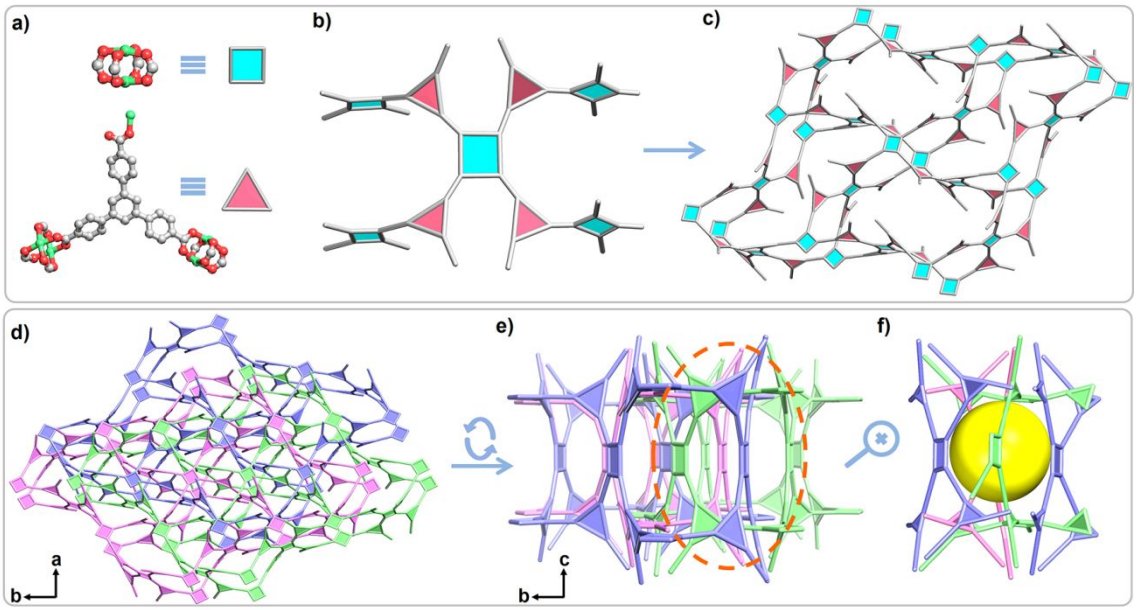

Figure S5. Structure of region A: topology simplification of the binuclear SBU (a) and the ligand (b), and the layer assembled by SBU-1 and BTB (c), 3-fold interpenetrated structure for region A with the cavity (d-f).

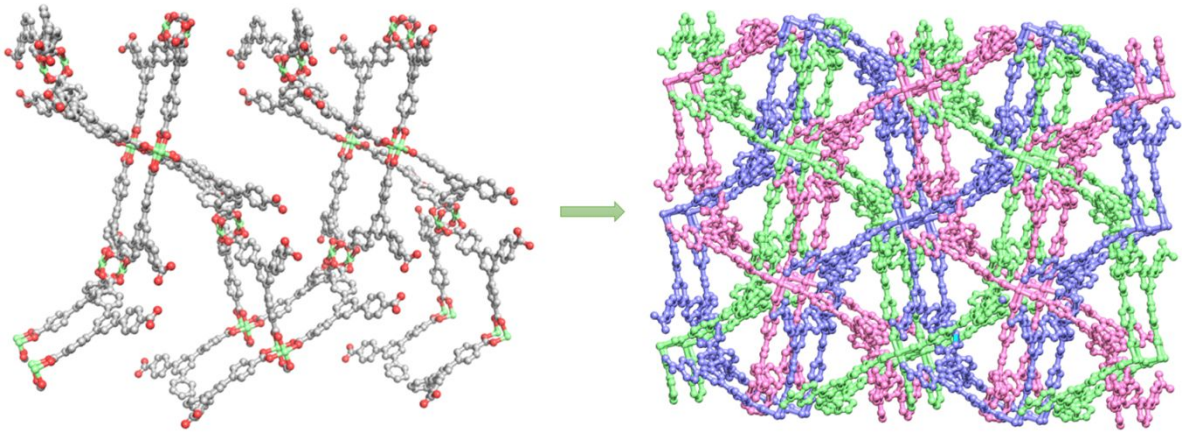

Figure S6. The layer assembled by SBU-1 and BTB (left); 3-fold interpenetrated structure (right).

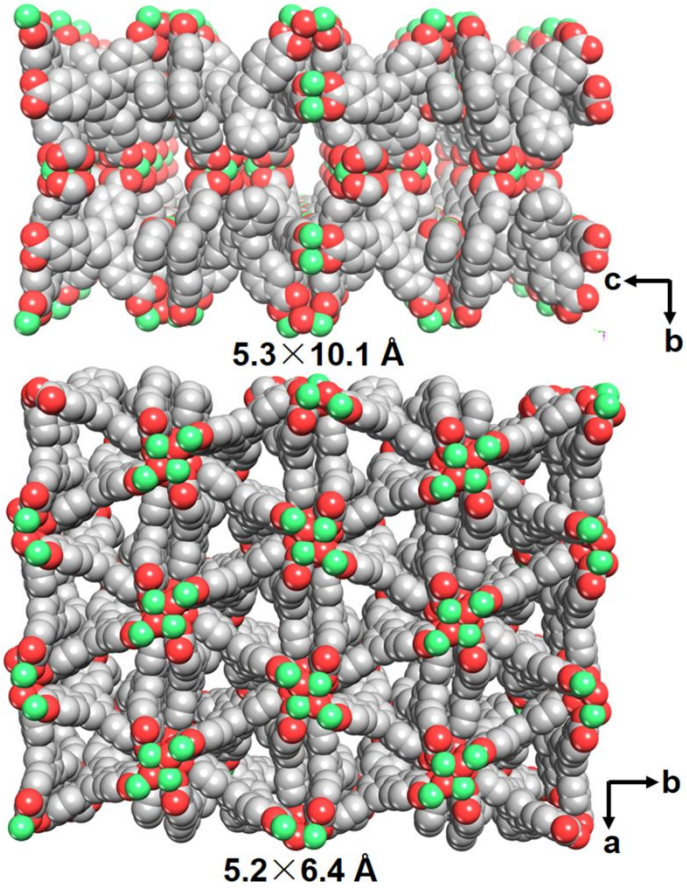

Figure S7. The illustration of multiple pores for region-A displayed by CPK model in different directions (regardless of van der Waals radii).

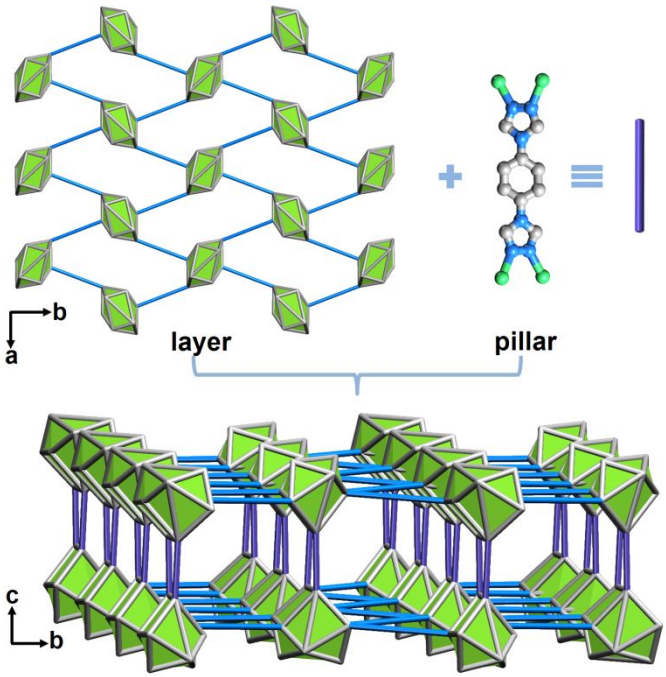

Figure S8. The square lattice layer assembled by SBU-2 and p-tr$_2$ph (top); pillared-layer view of the region B (bottom).

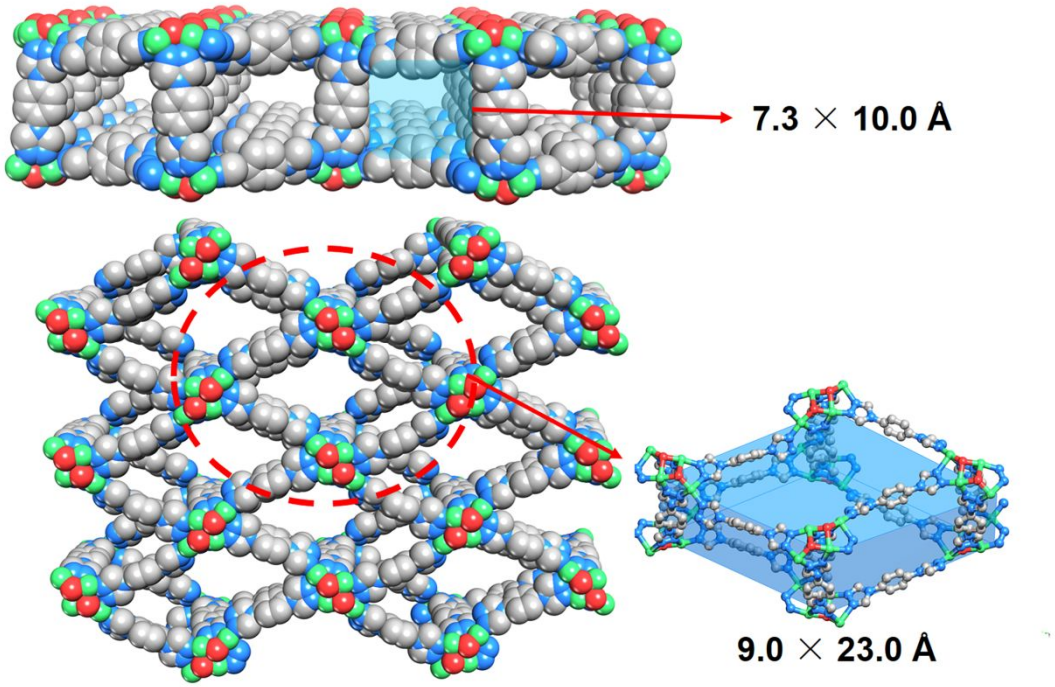

Figure S9. The illustration of multiple pores for region B displayed by CPK model in different directions (regardless of van der Waals radii).

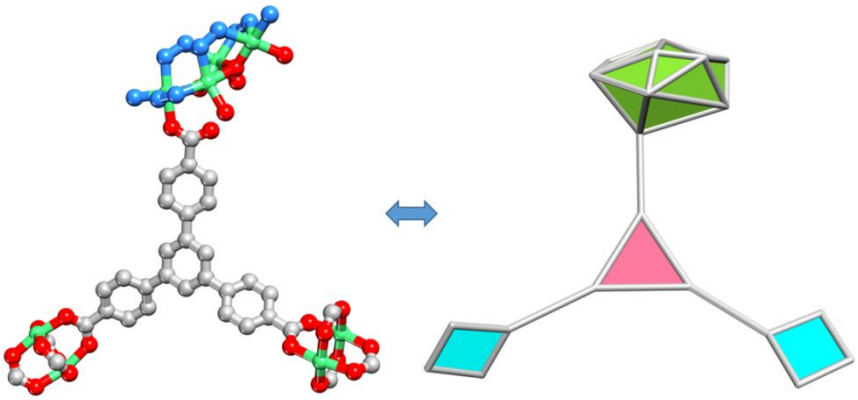

Figure S10. The BTB ligand connected with one SBU-1 and two SBU-2: ball and stick view (left), polyhedron view (right).

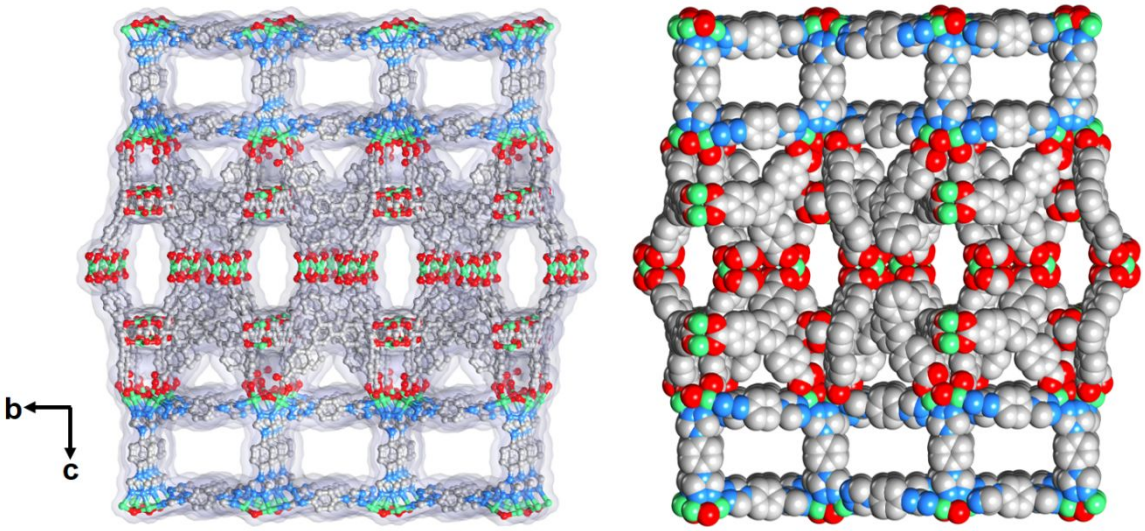

Figure S11. The illustration of multiple pores for **JLU-MOF107** displayed by Connolly surface areas (left) and CPK model (right).

FT-IR and optical image of JLU-MOF107

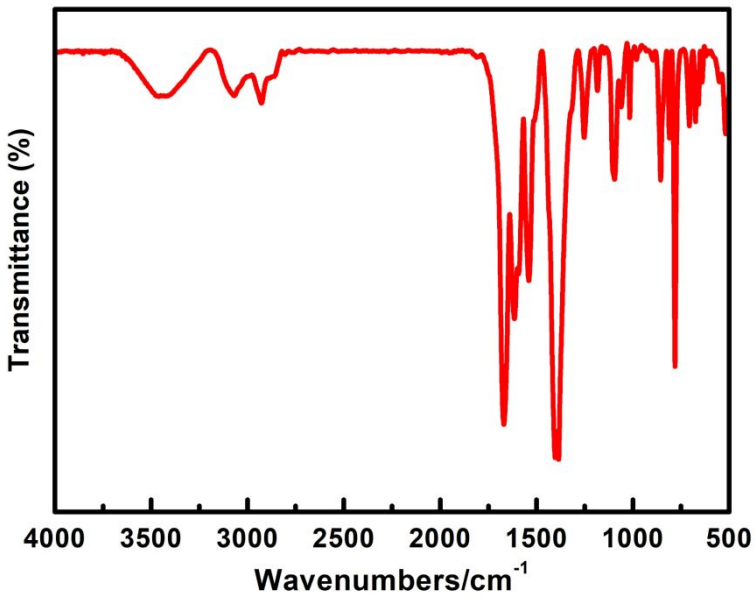

Figure S12. FT-IR spectrum of JLU-MOF107.

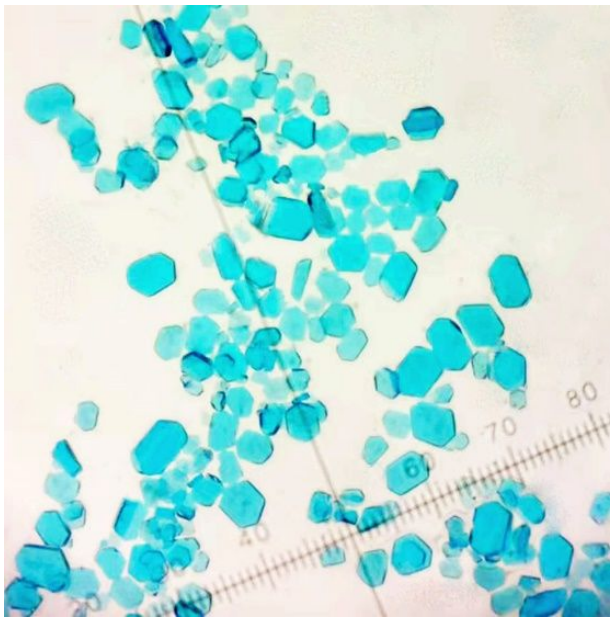

Figure S13. Single crystal optical images of JLU-MOF107.

PXRD and TGA of JLU-MOF107

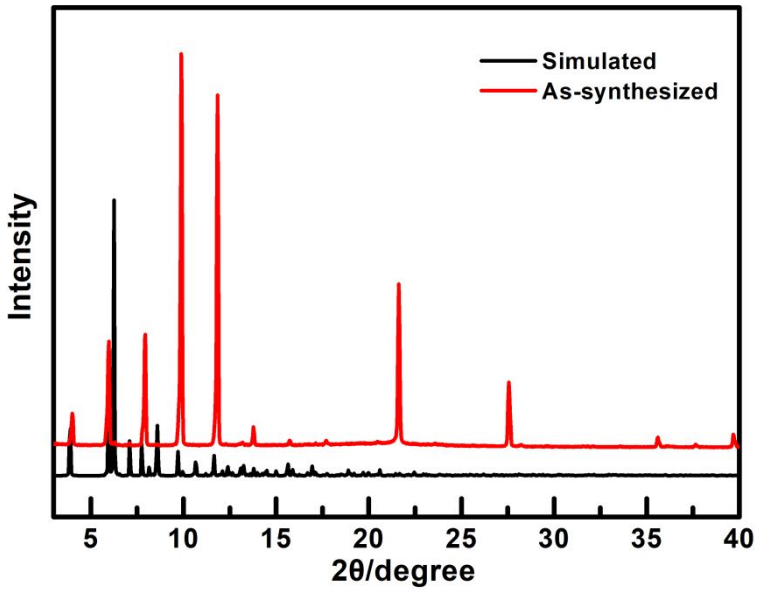

Figure S14. PXRD patterns of the simulated and as-synthesized JLU-MOF107.

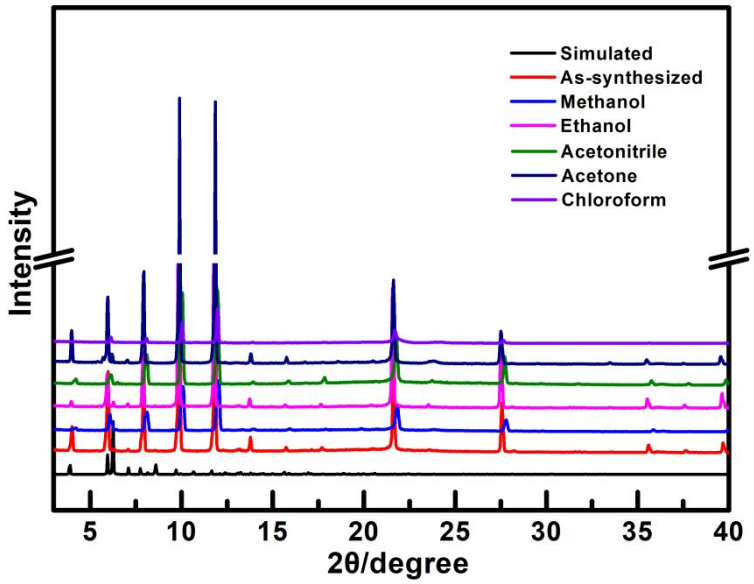

Figure S15. PXRD patterns of different solvent-exchanged JLU-MOF107 samples.

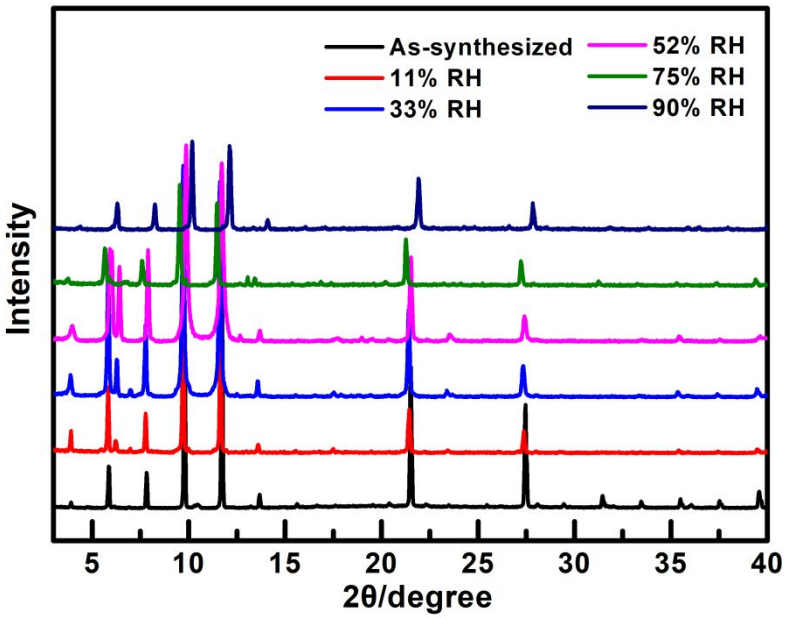

Figure S16. PXRD patterns of as-synthesized and exposed JLU-MOF107 under different relative humidity (RH) condition for 1 week.

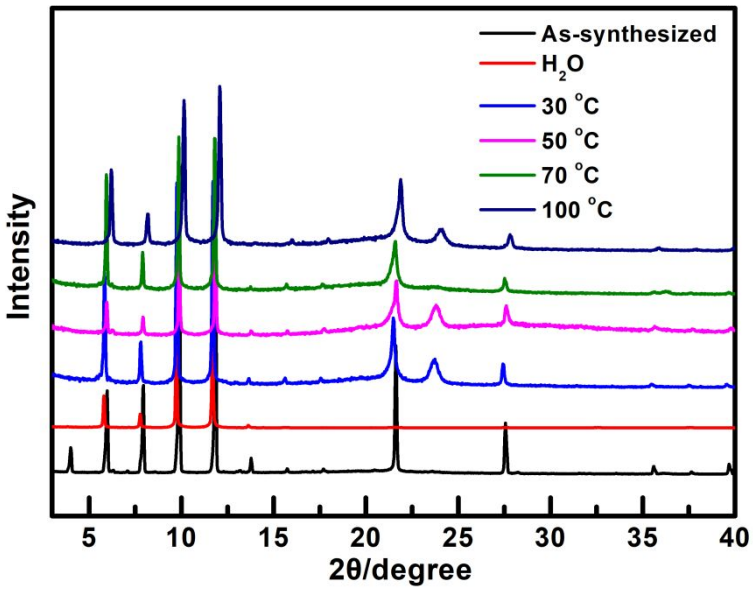

Figure S17. PXRD patterns of as-synthesized and immersed in water at different temperatures for JLU-MOF107.

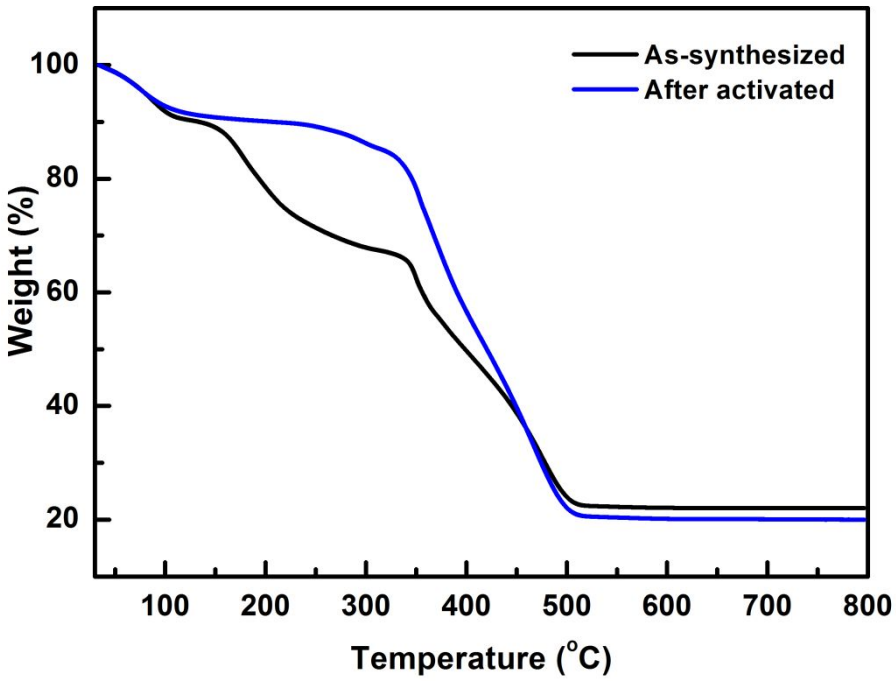

Figure S18. TGA curves of the as-synthesized and activated (acetonitrile exchanged) samples for JLU-MOF107.

Gas adsorption and separation behavior of JLU-MOF107

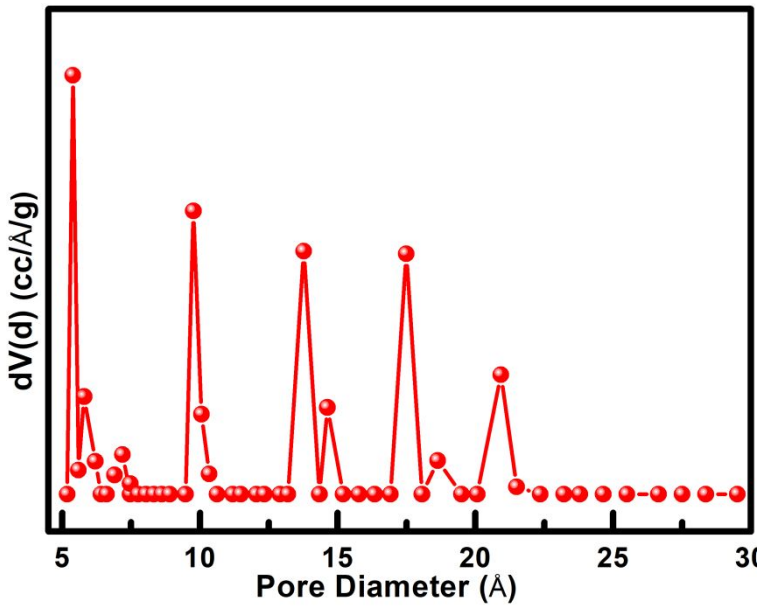

Figure S19. Pore size distribution plot of JLU-MOF107.

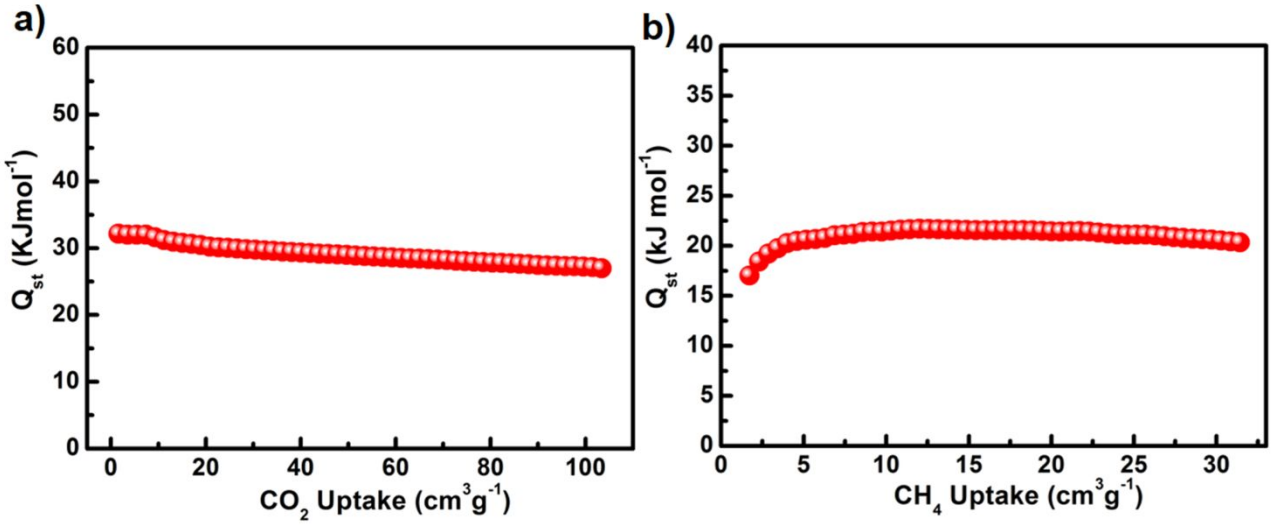

Figure S20. Q_{st} values calculated using the Clausius-Clapeyron equation of a) CO_2 and b) CH_4 for JLU-MOF107.

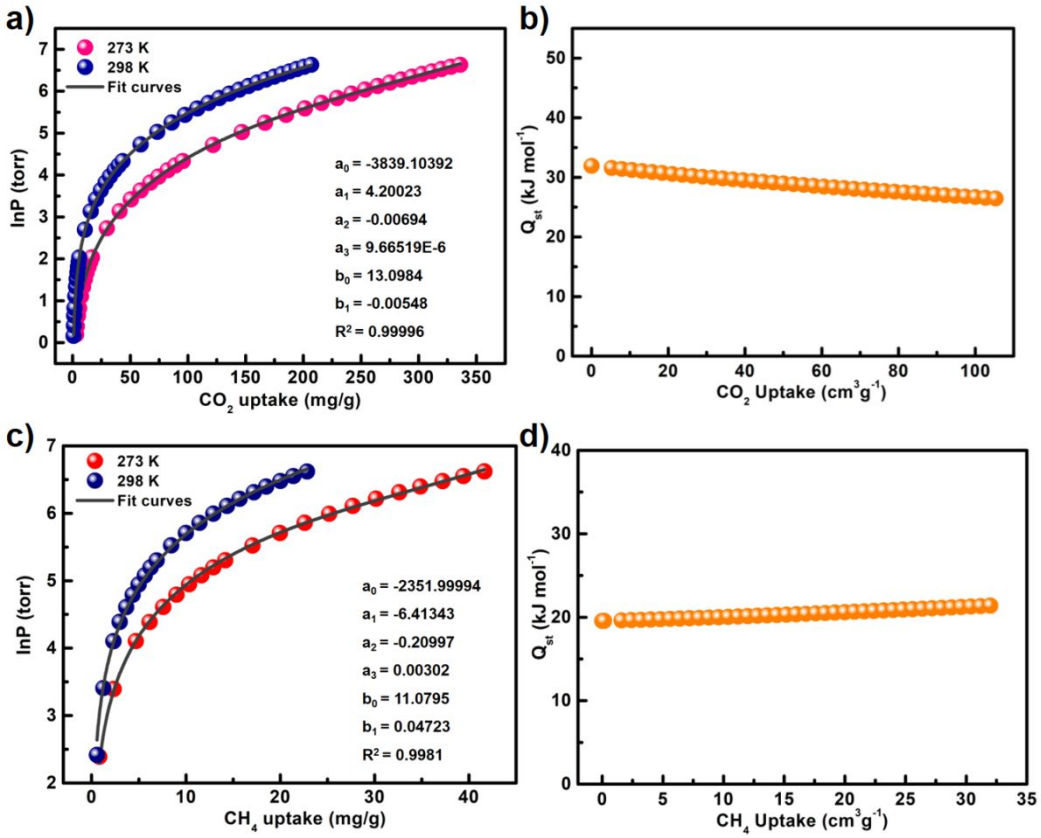

Figure S21. a) The fitting parameters of the virial model with the isotherms at 273 and 298 K for a) CO_2 and c) CH_4; Q_{st} values of b) CO_2 and d) CH_4.

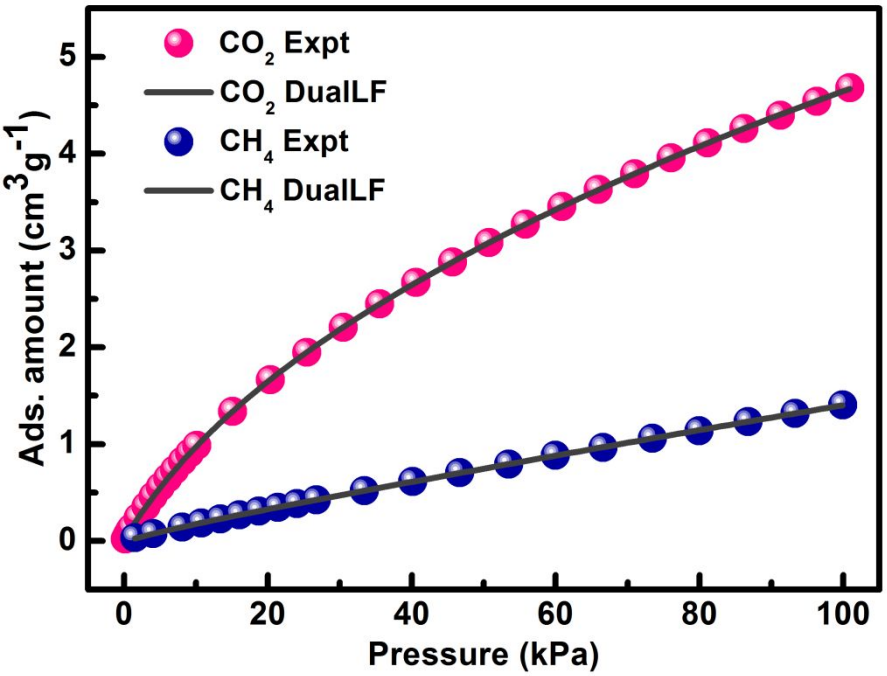

Figure S22. CO_2 and CH_4 isotherms at 298 K along with the dual-site Langmuir–Freundlich (DSLF) fits for JLU-MOF107.

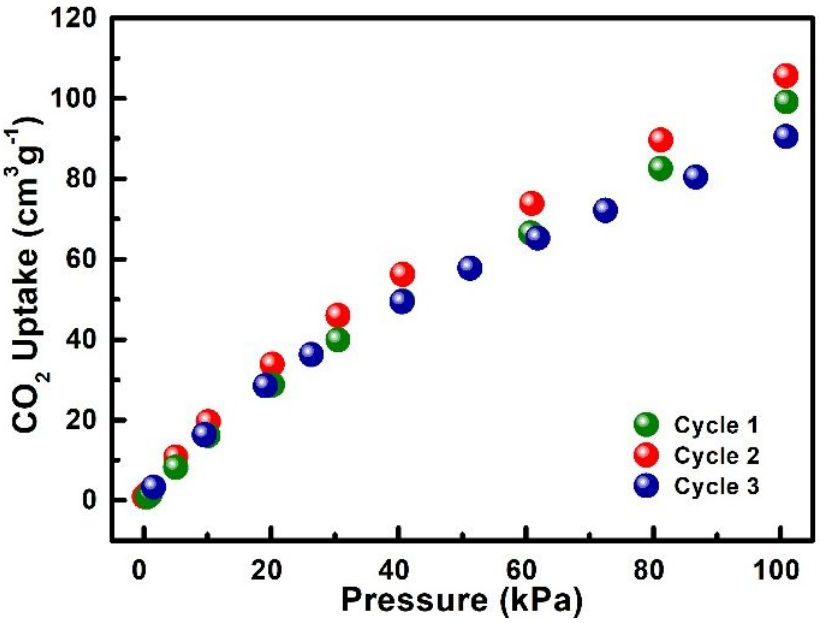

Figure S23. Three-cycle CO_2 adsorption tests at 298 K for JLU-MOF107.

S2. Calculation Procedures of IAST Selectivity

The measured experimental data is excess loadings (q^{ex}) of pure gas CO_2, CH_4 for **JLU-MOF107**, which should be converted to absolute loadings (q) firstly.

$$\boldsymbol{q = q^{ex} + \frac{pV_{pore}}{ZRT}} \qquad \text{Equation S1}$$

Here Z is the compressibility factor. The Peng-Robinson equation is used to estimate the value of Z to obtain the absolute loading, while the measured pore volume 0.55 $cm^3 \cdot g^{-1}$ (for **JLU-MOF107**) are necessary.

The dual-site Langmuir-Freundlich (DSLF) equation is used for fitting the isotherm data under 298 K.

$$\boldsymbol{q = q_{m_1} \times \frac{b_1 \times p^{1/n_1}}{1 + b_1 \times p^{1/n_1}} + q_{m_2} \times \frac{b_2 \times p^{1/n_2}}{1 + b_2 \times p^{1/n_2}}} \qquad \text{Equation S2}$$

Here p is the pressure of the bulk gas at equilibrium with the adsorbed phase (kPa), q is the adsorbed amount per mass of adsorbent ($mol \cdot kg^{-1}$), q_{m1} and q_{m2} are the saturation capacities of sites 1 and 2 ($mol \cdot kg^{-1}$), b_1 and b_2 are the affinity coefficients of sites 1 and 2 (1/kPa), n_1 and n_2 are the deviations from an ideal homogeneous surface.

The selectivity of preferential adsorption of component 1 over component 2 in a mixture containing 1 and 2, perhaps in the presence of other components too, can be formally defined as:

$$\boldsymbol{S = \frac{q_1/q_2}{p_1/p_2}} \qquad \text{Equation S3}$$

q_1 and q_2 are the absolute component loadings of the adsorbed phase in the mixture. These component loadings are also termed the uptake abilities. We calculate the values of q_1 and q_2 using the ideal adsorbed solution theory (IAST) of Myers and Prausnitz.

S3. Calculations of the Isosteric Heats of Gas Adsorption (Q_{st})

A virial-type[30] expression comprising the temperature-independent parameters a_i and b_j was employed to calculate the enthalpies of adsorption for CO_2 and CH_4 (at 273 and 298 K) on **JLU-MOF107**. In each case, the data were fitted using the equation:

$$ln^P = ln^N + {}^1/_T \sum_{i-0}^{m} a_i N^i + \sum_{j-0}^{n} b_j N^j \qquad \text{Equation S4}$$

Here, P is the pressure expressed in Torr, N is the amount adsorbed in mmol g^{-1}, T is the temperature in K, a_i and b_j are virial coefficients, m, n represent the number of coefficients required to adequately describe the isotherms (m and n were gradually increased until the contribution of extra added a and b coefficients was deemed to be statistically insignificant towards the overall fit, and the average value of the squared deviations from the experimental values was minimized). The values of the virial coefficients a_0 through a_m were then used to calculate the isosteric heat of adsorption using the following expression.

$$Q_{st} = -R \sum_{i-0}^{m} a_i N^i \qquad \text{Equation S5}$$

Q_{st} is the coverage-dependent isosteric heat of adsorption and R is the universal gas constant. The heat of gas sorption for **JLU-MOF107** in this manuscript are determined by using the sorption data measured in the pressure range from 0-1 bar (273 and 298 K for gases), which is fitted by the virial-equation very well.

S4. Theoretical Methods

Density functional theory (DFT) based calculations were performed to verify the vital roles of OMSs, LBS and N-polar sites to CO_2 affinity of the JLU-MOF107 skeleton. After a careful examination of the coordination of ligands with metal centers, two clusters with stoichiometry of $C_{28}H_{20}Cu_2O_8$ (2 Cu) and $C_{76}H_{64}Cu_4N_{18}O_{10}$ (4 Cu), respectively were truncated to mimic the CO_2 binding sites on skeleton of JLU-MOF107. 6-311g (d) basis set was used for main group elements,[1] while Lanl2dz effective core pseudopotential (ECP) was used for Cu.[2] ωB97XD functional that is capable to handle the long range dispersive interaction was used to calculate the CO_2 affinity.[3] This approach was previously used to interpret CO_2 adsorption in porous materials.[4-5] All the calculations were performed with Gaussian 16.[6] The CO_2 affinity (E_{ads}) was calculated as

$$E_{ads} = (E_{CO_2} + E_{Cluster}) - E_{Cluster+CO_2}$$

Equation S6

where E_{CO_2}, $E_{Cluster}$ and $E_{Cluster+CO_2}$ are the energy of free gaseous CO_2, optimized clusters, and adsorption structures, respectively.

S5. Supporting Tables

Table S1. Crystal data and structure refinements for JLU-MOF107.

Compound	JLU-MOF107
Formula	C_{140} H_{97} Cu_8 N_{18} O_{30}
Mw	3019.67
Temp (K)	200.0
Wavelength (Å)	0.71073
Crystal system	orthorhombic
Space group	*Ibam*
a (Å)	15.9884(4)
b (Å)	30.4807(6)
c (Å)	91.403(2)
α (°)	90
β (°)	90
γ (°)	90
V (Å^3)	44544.2(17)
Z, D_C (Mg/m^3)	8, 0.901
F(000)	12280
θ range (deg)	2.156 - 25.393
reflns collected/unique	152098 / 20555
R_{int}	0.0496
data/restraints/params	20555 / 260 / 946
GOF on F^2	1.038
R^1, wR^2 (I>2σ(I))	0.0428, 0.1200
R^1, wR^2 (all data)	0.0536, 0.1267

The B level alerts in the checkCIF file can be explained as following: O15-H15A/B and O87-H87A/B are both from axial water molecules of SBU-1 and there is no acceptor around them.

Summary of CO_2 (mmol g^{-1}) uptake at 273 K

Table S2. Summary of CO_2 (mmol g^{-1}) uptake from gas adsorption isotherms for various MOF materials at 273 K.

MOF	CO_2 uptake	Ref.
ZJU-12	10.6	7
Cu-TDPAT	10.1	8
JLU-Liu21	9.3	9
[Cu(Me-4py-trz-ia)]	9.2	10
$Cu_2(abtc)_3$	8.7	11
CPM-33b	7.8	12
CPM-733	7.6	13
JLU-Liu20	7.2	9
CPM-33a	6.1	12
$[Zn_2(abtc)(DMF)_2]_3$	4.6	11
SUMOF-2	4.3	14
UiO-66-AD4	3.6	15
LIFM-33	3.6	16
SNU-5	0.9	11
JLU-MOF107	**7.6**	**This work**

Summary of CO_2 (mmol g^{-1}) uptake at 298 K

Table S3. Summary of CO_2 uptake (mmol g^{-1}) from gas adsorption isotherms for various MOF materials at 298 K.

MOF	CO_2 uptake	Ref.
Li@HKUST-1	10.6	17
Ni-4PyC	8.2	18
CPO-27-Mg	7.1	19
MFU-4	5.7 (300 K)	20
CPM-33b	5.6	12
ZJU-12	5.5	7
JLU-Liu21	5.2	9
Zn($BPZNO_2$)	5	21
UTSA-16	4.4	22
NJU-Bai52	4.3	23
CALF-20	4.07	24
mmen-Mg_2(dobpdc)	3.9	25
bio-MOF-12	3.2	26
SHF-61	2.4	27
NH_2-MIL-53(Al)	1.5	28
JLU-MOF107	**4.7**	**This work**

References

1. Krishnan, R.; Binkley, J. S.; Seeger, R.; Pople, J. A. Self-Consistent Molecular-Orbital Methods. XX. A Basis Set for Correlated Wave-Functions. *J. Chem. Phys.* **1980**, *72*, 650-654.

2. Hay, P. J.; Wadt, W. R. Ab Initio Effective Core Potentials for Molecular Calculations - Potentials for the Transition-Metal Atoms Sc to Hg. *J. Chem. Phys.* **1985**, *82*, 270-283.

3. Chai, J. D.; Head-Gordon, M. Long-Range Corrected Hybrid Density Functionals with Damped Atom-Atom Dispersion Corrections. *Phys. Chem. Chem. Phys.* **2008**, *10*, 6615-6620.

4. Zhao, Y.; Liu, X.; Yao, K. X.; Zhao, L.; Han, Y. Superior Capture of CO_2 Achieved by Introducing Extra-framework Cations into N-doped Microporous Carbon. *Chem. Mat.* **2012**, *24*, 4725-4734.

5. Qiao, J.; Liu, X.; Liu, X.; Liu, X.; Zhang, L.; Liu, Y. Two Urea-Functionalized *pcu* Metal-Organic Frameworks Based on Pillared-Layer Strategy for Gas Adsorption and Separation. *Inorg. Chem. Front.* **2020**, *7*, 3500-3508.

6. Frisch, M. J.; Trucks, G. W.; Schlegel, H. B.; Scuseria, G. E.; Robb, M. A.; Cheeseman, J. R.; Scalmani, G.; Barone, V.; Petersson, G. A.; Nakatsuji, H.; Li, X.; Caricato, M.; Marenich, A. V.; Bloino, J.; Janesko, B. G.; Gomperts, R.; Mennucci, B.; Hratchian, H. P.; Ortiz, J. V.; Izmaylov, A. F.; Sonnenberg, J. L.; Williams; Ding, F.; Lipparini, F.; Egidi, F.; Goings, J.; Peng, B.; Petrone, A.; Henderson, T.; Ranasinghe, D.; Zakrzewski, V. G.; Gao, J.; Rega, N.; Zheng, G.; Liang, W.; Hada, M.; Ehara, M.; Toyota, K.; Fukuda, R.; Hasegawa, J.; Ishida, M.; Nakajima, T.; Honda, Y.; Kitao, O.; Nakai, H.; Vreven, T.; Throssell, K.; Montgomery Jr., J. A.; Peralta, J. E.; Ogliaro, F.; Bearpark, M. J.; Heyd, J. J.; Brothers, E. N.; Kudin, K. N.; Staroverov, V. N.; Keith, T. A.; Kobayashi, R.; Normand, J.; Raghavachari, K.; Rendell, A. P.; Burant, J. C.; Iyengar, S. S.; Tomasi, J.; Cossi, M.; Millam, J. M.; Klene, M.; Adamo, C.; Cammi, R.; Ochterski, J. W.; Martin, R. L.; Morokuma, K.; Farkas, O.; Foresman, J. B.; Fox, D. J. *Gaussian 16 Rev. C.01*, Wallingford, CT, 2016.

7. Duan, X.; Cui, Y.; Yang, Y.; Qian, G. A Novel Methoxy-Decorated Metal–Organic Framework Exhibiting High Acetylene and Carbon Dioxide Storage Capacities.

CrystEngComm **2017**, *19*, 1464-1469.

8. Li, B.; Zhang, Z.; Li, Y.; Yao, K.; Zhu, Y.; Deng, Z.; Yang, F.; Zhou, X.; Li, G.; Wu, H.; Nijem, N.; Chabal, Y. J.; Lai, Z.; Han, Y.; Shi, Z.; Feng, S.; Li, J. Enhanced Binding Affinity, Remarkable Selectivity, and High Capacity of CO_2 by Dual Functionalization of a rht-Type Metal–Organic Framework. *Angew. Chem., Int. Ed.* **2012**, *51*, 1412-1415.

9. Liu, B.; Yao, S.; Shi, C.; Li, G.; Huo, Q.; Liu, Y. Significant Enhancement of Gas Uptake Capacity and Selectivity via the Judicious Increase of Open Metal Sites and Lewis Basic Sites within Two Polyhedron-Based Metal–Organic Frameworks. *Chem. Comm.* **2016**, *52*, 3223-3226.

10. Lässig, D.; Lincke, J.; Moellmer, J.; Reichenbach, C.; Moeller, A.; Gläser, R.; Kalies, G.; Cychosz, K. A.; Thommes, M.; Staudt, R.; Krautscheid, H. A Microporous Copper Metal–Organic Framework with High H_2 and CO_2 Adsorption Capacity at Ambient Pressure. *Angew. Chem., Int. Ed.* **2011**, *50*, 10344-10348.

11. Lee, Y.-G.; Moon, H. R.; Cheon, Y. E.; Suh, M. P. A Comparison of the H_2 Sorption Capacities of Isostructural Metal–Organic Frameworks with and without Accessible Metal Sites: $[\{Zn_2(abtc)(dmf)_2\}_3]$ and $[\{Cu_2(abtc)(dmf)_2\}_3]$ versus $[\{Cu_2(abtc)\}_3]$. *Angew. Chem., Int. Ed.* **2008**, *47*, 7741-7745.

12. Zhao, X.; Bu, X.; Zhai, Q.-G.; Tran, H.; Feng, P. Pore Space Partition by Symmetry-Matching Regulated Ligand Insertion and Dramatic Tuning on Carbon Dioxide Uptake. *J. Am. Chem. Soc.* **2015**, *137*, 1396-1399.

13. Wang, Y.; Jia, X.; Yang, H.; Wang, Y.; Chen, X.; Hong, A. N.; Li, J.; Bu, X.; Feng, P. A Strategy for Constructing Pore-Space-Partitioned MOFs with High Uptake Capacity for C_2 Hydrocarbons and CO_2. *Angew. Chem., Int. Ed.* **2020**, *59*, 19027-19030,

14. Yao, Q.; Su, J.; Cheung, O.; Liu, Q.; Hedin, N.; Zou, X. Interpenetrated Metal–Organic Frameworks and Their Uptake of CO_2 at Relatively Low Pressures. *J. Mater. Chem.* **2012**, *22*, 10345-10351.

15. Hong, D. H.; Suh, M. P. Enhancing CO_2 Separation Ability of a Metal–Organic Framework by Post-Synthetic Ligand Exchange with Flexible Aliphatic Carboxylates. *Chem. - Eur. J.* **2014**, *20*, 426-434.

16. Chen, C.-X.; Wei, Z.; Jiang, J.-J.; Fan, Y.-Z.; Zheng, S.-P.; Cao, C.-C.; Li, Y.-H.;

Fenske, D.; Su, C.-Y. Precise Modulation of the Breathing Behavior and Pore Surface in Zr-MOFs by Reversible Post-Synthetic Variable-Spacer Installation to Fine-Tune the Expansion Magnitude and Sorption Properties. *Angew. Chem., Int. Ed.* **2016**, *55*, 9932-9936.

17. Xiang, Z.; Hu, Z.; Cao, D.; Yang, W.; Lu, J.; Han, B.; Wang, W. Metal–Organic Frameworks with Incorporated Carbon Nanotubes: Improving Carbon Dioxide and Methane Storage Capacities by Lithium Doping. *Angew. Chem., Int. Ed.* **2011**, *50*, 491-494.

18. Nandi, S.; Luna, P. De; Daff Thomas, D.; Rother, J.; Liu, M.; Buchanan, W.; Ayman, I. Hawari; Tom, K. Woo; Vaidhyanathan, R. A Single-Ligand Ultra-Microporous MOF for Precombustion CO_2 Capture and Hydrogen Purification. *Sci. Adv.* **2015**, 1, 1500421.

19. Valenzano, L.; Civalleri, B.; Sillar, K.; Sauer, J. Heats of Adsorption of CO and CO_2 in Metal–Organic Frameworks: Quantum Mechanical Study of CPO-27-M (M = Mg, Ni, Zn). *J. Phys. Chem. C*. **2011**, *115*, 21777-21784.

20. Cai, Z.; Bien, C. E.; Liu, Q.; Wade, C. R. Insights into CO_2 Adsorption in M–OH Functionalized MOFs. *Chem. Mater.* **2020**, *32*, 4257-4264.

21. Mosca, N.; Vismara, R.; Fernandes, J. A.; Tuci, G.; Nicola, C. Di; Domasevitch, K. V.; Giacobbe, C.; Giambastiani, G.; Pettinari, C.; Aragones-Anglada, M.; Moghadam, P. Z.; Fairen-Jimenez, D.; Rossin, A.; Galli, S. Nitro-Functionalized Bis(Pyrazolate) Metal–Organic Frameworks as Carbon Dioxide Capture Materials Under Ambient Conditions. *Chem. - Eur. J.* **2018**, *24*, 13170-13180.

22. Masala, A.; Vitillo, J. G.; Mondino, G.; Grande, C. A.; Blom, R.; Manzoli, M.; Marshall, M.; Bordiga, S. CO_2 Capture in Dry and Wet Conditions in UTSA-16 Metal–Organic Framework. *ACS Appl. Mater. Interfaces.* **2017**, *9,* 455-463.

23. Song, X.; Zhang, M.; Chen, C.; Duan, J.; Zhang, W.; Pan, Y.; Bai, J. Pure-Supramolecular-Linker Approach to Highly Connected Metal–Organic Frameworks for CO_2 Capture. *J. Am. Chem. Soc.* **2019**, *141*, 14539-14543.

24. Lin, J.-B.; Nguyen, T. T. T.; Vaidhyanathan, R.; Burner, J.; Taylor, J. M.; Durekova, H.; Akhtar, F.; Mah, R. K.; Ghaffari-Nik, O.; Marx, S.; Fylstra, N.; Iremonger, S. S.; Dawson, K. W.; Sarkar, P.; Hovington, P.; Rajendran, A.; Woo, T. K.; Shimizu, G. K. H. A Scalable Metal-Organic Framework as a Durable Physisorbent for Carbon Dioxide Capture. *Science* **2021**, *374*, 1464-1469.

25. McDonald, T. M.; Lee, W. R.; Mason, J. A.; Wiers, B. M.; Hong, C. S.; Long, J. R. Capture of Carbon Dioxide from Air and Flue Gas in the Alkylamine-Appended Metal–Organic Framework mmen-Mg_2(dobpdc), *J. Am. Chem. Soc.* **2012**, *134*, 7056-7065.

26. Li, T.; Chen, D.-L.; Sullivan, J. E.; Kozlowski, M. T.; Johnson, J. K.; Rosi, N. L. Systematic Modulation and Enhancement of $CO_2 : N_2$ Selectivity and Water Stability in an Isoreticular Series of Bio-MOF-11 Analogues, *Chem. Sci.* **2013**, *4*, 1746-1755.

27. Carrington, E. J.; McAnally, C. A.; Fletcher, A. J.; Thompson, S. P.; Warren, M.; Brammer, L. Solvent-Switchable Continuous-Breathing Behaviour in a Diamondoid Metal–Organic Framework and its Influence on CO_2 versus CH_4 Selectivity, *Nat. Chem.* **2017**, *9*, 882-889.

28. Couck, S.; Denayer, J. F. M.; Baron, G. V.; Rémy, T.; Gascon, J.; Kapteijn, F. An Amine-Functionalized MIL-53 Metal−Organic Framework with Large Separation Power for CO_2 and CH_4, *J. Am. Chem. Soc.* **2009**, *131*, 6326-6327.